



# Hysteretic Behavior of Rubber Bearing with Yielding Shear Devices

Mahdi Saadatnia<sup>1</sup> · Hossein Tajmir Riahi<sup>2</sup>  · Mohsen Izadinia<sup>1</sup>

Received: 24 October 2017 / Accepted: 27 August 2018 / Published online: 3 September 2018  
© Korean Society of Steel Construction 2018

## Abstract

Using the perforated yielding shear plates as an energy dissipated device instead of lead core in rubber bearing is assessed in this paper. The advantage of this innovative isolator compared to lead rubber bearing is the ability of being replaced easily and its less displacement with high ability of energy dissipation. Three different isolators with perforated shear plates with hole cross-section of 15%, 18%, and 33% of cross-sectional of plate surface area are investigated. Three types of shear plates of 2, 3 and 4 mm thicknesses made of two types of steel with different yield stress are assessed. By decreasing the shear plate thickness and increasing the number of the plate holes and selecting the shear plate with lower yield stress, the effective stiffness and the amount of energy dissipation and lateral force in the isolator are reduced. Changing shear plate thickness and number of holes do not affect the viscous damping, while increasing the plate yield stress increases viscous damping. Therefore the choice of the shear plate with appropriate thickness, number of holes and plate yield stress can lead to an isolator with acceptable behavior. The suggested isolator can achieve similar characteristics of lead rubber bearing at 50% shear strain and therefore its design basics should be defined differently rather than lead rubber bearing.

**Keywords** Perforated yielding shear plates · Base-isolation · Cyclic behavior · Energy dissipation · Lead rubber bearing

## 1 Introduction

Seismic-base-isolation of buildings and bridges is one of the most commonly adopted methods in controlling structures against sever earthquakes. This method is usually divided into two groups of rubber bearing and friction pendulum bearing. The record of seismic-base-isolation is provided by Warn and Ryan (2012). Rubber bearing consist of: natural rubber bearings (NRBs) (Iizuka 2000; Sanchez et al. 2012) lead rubber bearing (LRB) (Ghobarah and Ali 1990; Ryan et al. 2005) and high-damping rubber (HDR) bearing (Bhuiyan et al. 2009). A method considered in seismic-base-isolation design is the transition of fundamental natural period of a structure into a greater period. In this method, the behavior of the superstructure is mostly of linear nature. The base isolation, in addition to having the ability to move, must be

equipped by the means of an energy dissipation device to prevent large displacements.

In a LRB, lead core is considered as an energy dissipater which provides the necessary damping for the bearing. In a HDR bearing, additional materials are injected into the rubber to provide the necessary damping for bearing. In severe ground motion, the lead in the rubber bearing undergoes deformation (Paul 2016) and loses its efficiency. Because the core of lead is located in the interconnected layers of rubber and steel, it is hard to replace it. In HDR bearings, the high deformation of rubber and its cyclic behavior in strong earthquakes can damage the rubber and ultimately change the entire bearing.

There exist many studies on the energy-dissipating devices application other than lead core in rubber bearing. For example the U-shaped damper is used in rubber bearing to stabilize the hysteretic response with large deformation (Oh et al. 2013). In another study Dezfuli and Alam (2013, 2015), applied shape memory alloy (SMA) wire as a damper in rubber bearing which can restore the initial form after being deformed. Dezfuli et al. (2017) have assessed the effect of (SMA-LRB) on bridges. Applying SMA in this study lead to an increase in the horizontal stiffness of bearing which has reduced the strain demand of LRB and

✉ Hossein Tajmir Riahi  
tajmir@eng.ui.ac.ir

<sup>1</sup> Department of Civil Engineering, Najafabad Branch, Islamic Azad University, Najafabad, Iran

<sup>2</sup> Department of Civil Engineering, University of Isfahan, Isfahan, Iran

the displacement of the bridge deck. In another study Dezfouli and Alam (2017), application of SMA–LRB on bridges reduced strain demand by 46% and increased energy dissipation by about 31% compared to the LRB. Wall damping system with steel damping is proposed and tested by Ahn et al. (2016). This device could not only provide good seismic performance but could also be easily repaired after an earthquake. Shear panel dampers (SDPs) installed in frame bridges piers are assessed by Ge et al. (2012) and the sensitivity of two quantities of the SPD's capacity (maximum shear deformation and cumulative in elastic deformation) is studied.

The yielding shear devices (YSD) are another type of dampers that are mostly applied on top of an inverted-V brace (Chan et al. 2009). YSD is located in a hollow section which provides a continuous support to the diaphragm plate and at the same time provides an interface to connect to the main structure. Due to the slenderness of these plates, they tend to buckle out-of-plane and produce pinched hysteresis. High initial stiffness and low yield stress are their two unique properties compared to the flexural and axial yielding of steel components. The stiffness of these plates controls the structure movement.

In this study, shear plates are applied instead of lead core in a rubber bearing. These shear plates are welded on the four sides of the isolator to the top and bottom steel plates of the bearing. Because of the need for minimal displacement in the bearing, perforated yielding shear devices (PYSD) are applied. The stiffness of PYSD (Chan et al. 2013; Formisano et al. 2016) is reduced in relation to the non-perforated shear plates and the plate displacement increases before rupturing.

First, experimental models of a LRB and a PYSD are assessed numerically using finite element method (FEM). This is done by obtaining the cyclic behavior of LRB and PYSD and comparing the results with the experimental results and finally the accuracy of the numerical models is obtained. Next, by removing the lead core and adding the perforated shear plates to the bearing, the cyclic behavior of the displacement force of the new bearing is obtained. Then, in addition to effective stiffness, the energy dissipation and equivalent viscous damping of the bearing is obtained and compared for LRB and PYSD bearing. Finally, the effects of steel plate thickness, mechanical properties and the percentage of plate perforation on the special characteristics of the bearing are analyzed and examined.

## 2 Formulation of YSD

YSDs were first examined (Williams and Albermani 2003; Chan et al. 2009) on top of inverted-V braces. This device consists of a square-shaped plate welded into a box at its edges. Compared to other dampers, the shear plates

have high elastic stiffness, which is considered important in controlling the relative displacement of floors. Yield strength is obtained according to von Mises criterion from the following equation:

$$F_y = \frac{f_y}{\sqrt{3}} dt \quad (1)$$

where  $d$  is the width of the steel plate and  $t$  is the thickness of diaphragm plate and  $f_y$  is its tensile yield stress. For a device with a slender diaphragm plate, elastic shear buckling occurs prior to yielding. The critical shear stress  $\tau_{cr}$  is obtained by the following equation:

$$\tau_{cr} = k_s \frac{\pi^2 E}{12(1-\nu^2)} \left(\frac{t}{d}\right)^2 \quad (2)$$

where  $t$ ,  $d$ ,  $E$ ,  $\nu$  are the thickness, the width of the steel plate, the modulus of elasticity and the Poisson's ratio of the shear plate respectively. According to the theory (Roberts and Sabouri-Ghomi 1992), for square shape steel plates, the shear capacity and stiffness of the plates are obtained, through the following equations, respectively:

$$F_{wu} = bt \left( \tau_{cr} + \frac{1}{2} \sigma_{ty} \sin 2\theta \right) \quad (3)$$

$$K_w = \frac{\left( \tau_{cr} + \frac{1}{2} \sigma_{ty} \sin 2\theta \right)}{\left( \frac{\tau_{cr}}{G} + \frac{2\sigma_{ty}}{E \sin 2\theta} \right)} t \quad (4)$$

where  $b$  and  $G$ , are the length of steel plate and its shear modulus, respectively. The tension field stress develops on YSD with an angle  $\theta$  with horizontal orientation of the plate, Fig. 1. Components of stress in different directions are shown in Fig. 1 and used in Eqs. 3 and 4.

Sometimes due to the shear plate with excessive thickness, application of perforated shear plates becomes necessary. There also exist numerical and experimental studies on PYSD to achieve proper stiffness and strength for this device. For PYSDs, a decreasing coefficient  $\left(1 - \frac{A}{A_0}\right)$  is

proposed for Eqs. 3 and 4 (Formisano et al. 2016), where  $A$  is the opening area and  $A_0$  is the plate area. Vian et al. (2009) studied the strength and stiffness of perforated shear walls. Purba and Bruneau (2009) run numerical studies to provide an appropriate equation for the design of perforated shear walls. Valizadeh et al. (2012) run an experimental study to assess the effect of holes and slenderness ratio of plates on the shear behavior of seismic steel walls. De Matteis et al. (2016) run an experimental study to optimize the PYSD performance.

**Fig. 1** **a** Onset of buckling, **b** post-buckling tension field (Chan et al. 2013)

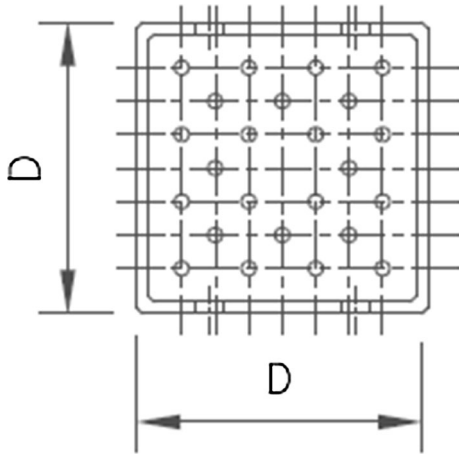
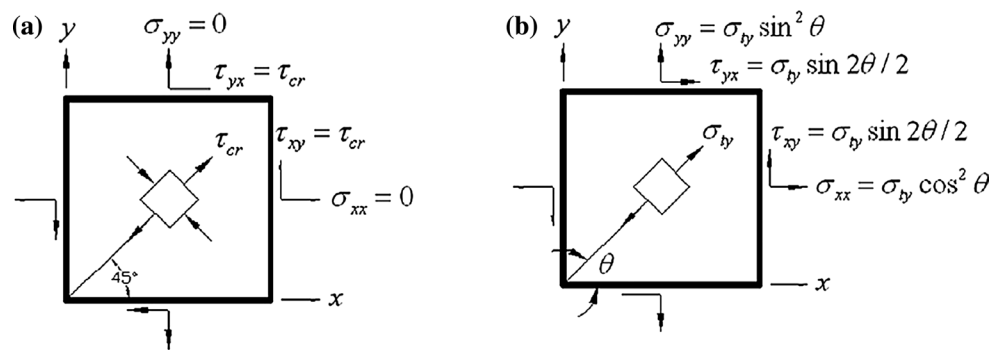


**Fig. 2** Perforated yielding shear device (Chan et al. 2013)

### 3 Verification

#### 3.1 PYSD Verification

Experimental studies are run on three types of (PYSD) by Chan et al. (2013). By choosing one of these plates and modeling it in Abaqus software and comparing the numerical results thereof with the experimental study, the validity of this newly proposed model is examined.

The selected shear plate is 3 mm thick welded inside a short length square hollow section. The square hollow section thickness is 4 mm and the side length shown in Fig. 2 with  $D$ , is 100 mm. The edges of the shearing plate are welded into the inner space of the square hollow section. The diameter of the holes in the plate is 5.5 mm. This plate is modeled through C3D8R solid elements in the Abaqus software. Running sensitivity analysis, it is revealed that 5 mm dimension is appropriate for the elements size. Material properties are assumed to be elastic-perfectly plastic with yield stress of 320 MPa of Mises plasticity. An elasto-plastic behavior with kinematic hardening is considered for steel to perform numerical simulation in the cyclic field. By restraining the degrees of

freedom at the lower surface of the box, the bottom of the shear plate remains constant and the upper surface moves under a specific loading protocol. There exists an initial imperfection in these plates caused by manufacturing or installing processes. This is assigned in the model by an initial out-of-plane imperfection proportional to the first buckling mode with amplitude of 1 mm. The comparison between experimental and numerical deformation of a sample tested by Chan et al. (2013) is shown in Fig. 3. The experimental-to-numerical comparison in terms of both hysteretic curves is shown in Fig. 4. The vertical axis of this diagram shows the normalized shear force through yield strengths and the horizontal axis of the shear strain of the plate. Numerical and experimental results reveal acceptable adaptation.

#### 3.2 LRB Verification

Abe et al. (2004) have run studies on an experimental sample of LRB illustrated in Fig. 5. The bearings designed to have a size of one-third of the real bearings installed at a highway bridge in Japan. Detailed design components of the bearings are tabulated in Table 1.

The bearing shown in Fig. 5 is modeled in Abaqus software. The natural rubber used in this bearing has viscous damping ratios about 2–3%. Neo hook model (Asl et al. 2014) is adopted for modeling rubber. The hybrid C3D8H element is applied to model rubber. The lead is modeled with 16 MPa Young modulus and 10 MPa yield stress and considered to have a bilinear kinematic hardening behavior. Steel plates are assumed to be isotropic material with a Young modulus of 210 MPa and a Poisson's ratio of 0.3. The C3D8R element is applied to model these plates. By assuming that the 7 MPa vertical stress is applied to the bearing, cyclic behavior of isolator is obtained for shear strains of 50% and 150% of the rubber. A comparison of this cyclic behavior of the numerical model with the experimental sample indicates the accuracy of the numerical results, (Fig. 6).

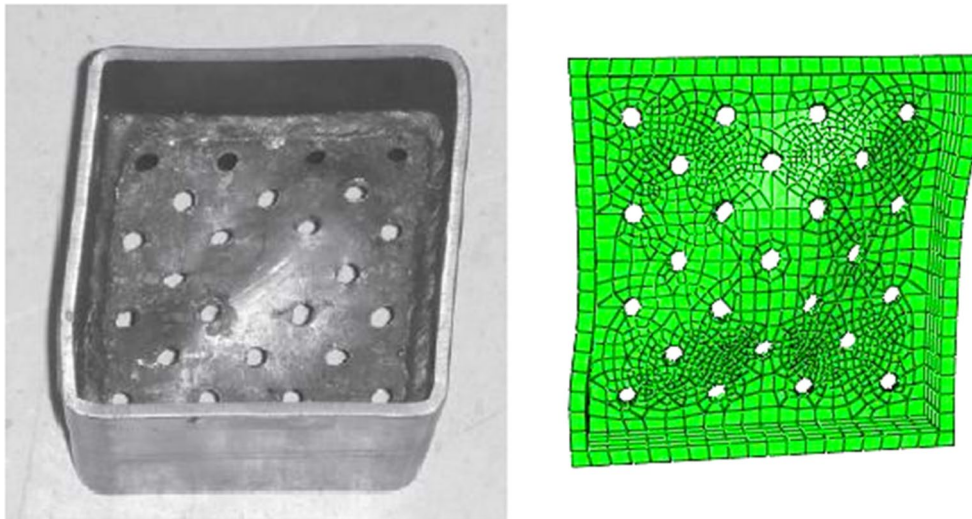
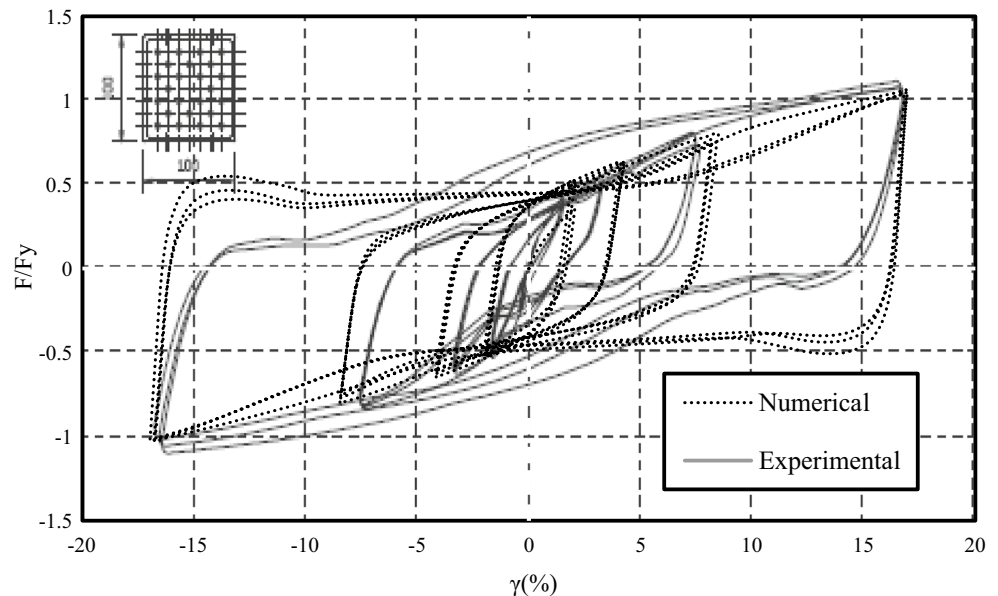


**Fig. 3** Experimental-numerical comparison in terms of deformed shape for the PYSD specimen tested by Chan et al. (2013)

**Fig. 4** Numerical calibration of experimental results on the PYSD specimen tested by Chan et al. (2013)



#### 4 Description of the Proposed FEM Model

Since PYSDs are the subject of discussion of this study, the lead core of the LRB introduced in the previous section is removed and these plates replace it. As the vertical distance of the upper and lower steel plates is 92.8 mm, the shear plate dimensions are considered as square of 92.8 mm. These plates are arranged on both sides of the bearing, in a symmetrical manner (Fig. 7a). To minimize analysis time, half of the bearing together with the shear plate is modeled in one direction. Since the flexural strength of the shear plate in other directions is negligible

in comparison with the original direction, the shear plate in the bearing is examined in one direction. Three types of perforated shear plates accompanied with the bearing are considered, (Fig. 7b).

The percentage of holes in PYSD1 (Type1), PYSD2 (Type2) and PYSD3 (Type3) are about 15%, 18% and 33% cross-section of shear plate, respectively. Shear plates are modeled by the C3D8R element. The mechanical properties of these plates are assumed as a bilinear model with kinematic plastic behavior. Three types of shear plates of 2, 3 and 4 mm thicknesses are assessed for the bearing. Two yield stresses of 240 MPa (st37 type) and 360 MPa (st52 type) are considered for the plates. Effects

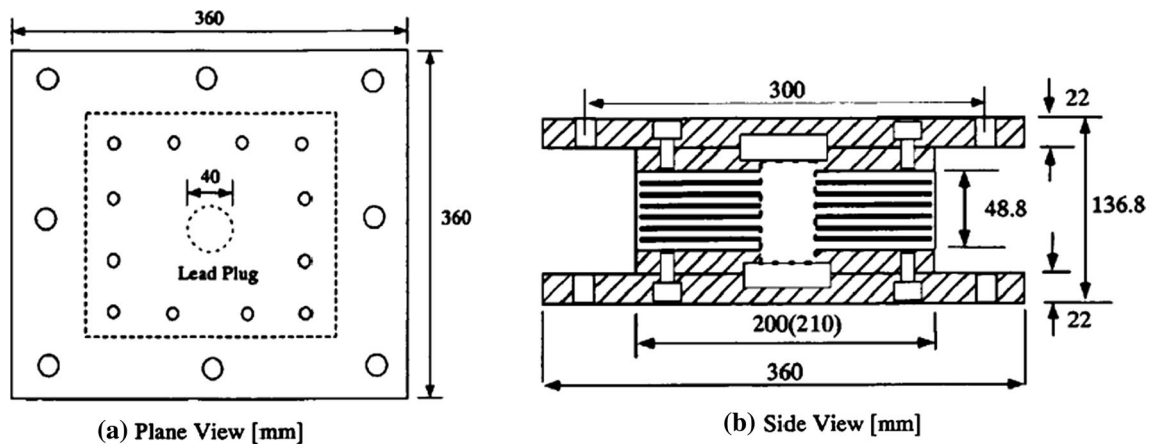


Fig. 5 Size of laminated rubber bearing used in experiments (Abe et al. 2004)

Table 1 Size of the Laminated Rubber Bearings

| Type of bearing                      | Lead rubber bearing |
|--------------------------------------|---------------------|
| Cross-section (mm)                   | 200 × 200           |
| Shear modulus (MPa)                  | 0.78                |
| Number of layers rubber              | 7                   |
| Thickness of one layer rubber (mm)   | 5                   |
| Number of inner steel plates         | 6                   |
| Thickness of inner steel plates (mm) | 2.3                 |
| Diameter of lead plug (mm)           | 40                  |

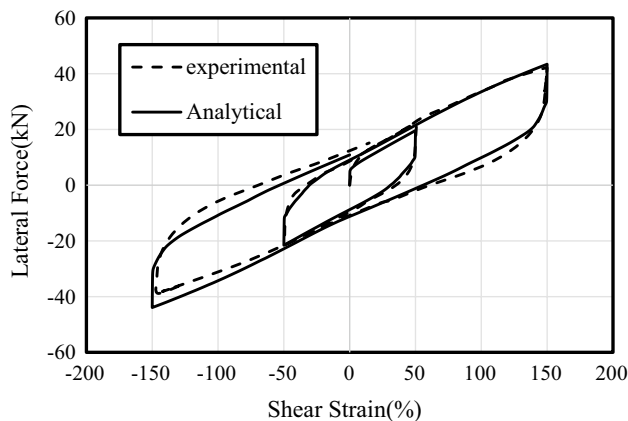


Fig. 6 Comparison of numerical and experimental hysteresis of LRB at 50% and 150% shear strains (Abe et al. 2004)

of different parameters of PYSD on the performance of the bearings are discussed in the next section. Name of the bearings introduce their specifications. As an example, the PYSD1-st37-t2 is Type 1 PYSD with a thickness of 2 mm for the plates and assuming st37 material type.

### 5 Discussion and Results

In order to assess the hysteresis behavior of bearings, horizontal stiffness, energy dissipation (energy dissipated per cycle, EDC), equivalent viscous damping ( $\beta$ ) and lateral forces in each cycles are investigated. The effective horizontal stiffness of the elastomeric isolator subjected to a specific shear strain amplitude is obtained from Eq. 5 (Naeim and Kelly 1999):

$$K_{H_{eff}}(\gamma) = \frac{F_{max} - F_{min}}{\Delta_{max} - \Delta_{min}} \tag{5}$$

where  $F_{max}$  and  $F_{min}$  are the maximum and minimum shear forces in the direction of the horizontal cyclic loading, respectively. Symbol  $\Delta_{max}$  and  $\Delta_{min}$  are the maximum and minimum lateral displacements, respectively. The equivalent viscous damping is obtained through the following equation:

$$\beta = \frac{EDC}{4\pi U_r} \tag{6}$$

where EDC is the dissipated energy per cycle equal to the area inside the lateral force–deflection hysteresis curve in each cycle.  $U_r$  is the restored (elastic) energy in the rubber bearing, which can be measured through Eq. (7) (Toopchi-Nezhad et al. 2008).

$$U_r = \frac{1}{2} K_{H_{eff}} \bar{\Delta}_{max}^2 \tag{7}$$

In which

$$\bar{\Delta}_{max} = \frac{\Delta_{max} + |\Delta|_{min}}{2} \tag{8}$$

The lateral force transferred to the structure on the isolator in each loading cycle is obtained through the following equation:

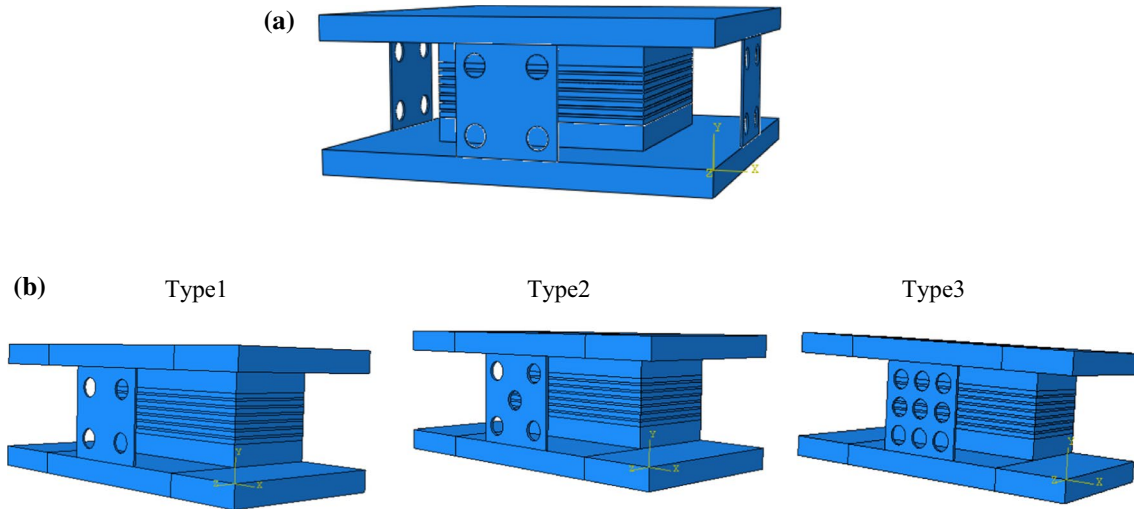


**Fig. 7** **a** Full view of the bearing with perforated shear plates, **b** half of the three types of rubber bearing accompanied with a perforated shear plate

$$F = K_{H_{eff}} \bar{\Delta}_{max} \quad (9)$$

Shear plates do not exhibit high displacement due to their high initial stiffness in comparison to the lead core. Since the dimensions of the shear plates considered in the isolator are similar to that of the shear damper tested in the V curved bracket, the maximum displacement of this shear plate is 1.75 cm. This displacement is approximately equal to 50% of the shear strain of the laminated rubber. For this purpose, protocol load for the rubber bearing with shear plate is considered in accordance with BSI BS EN 15129 for 10, 20 and 50% of the shear strain of the rubber. The LRB tested by Abe et al. (2004) is assessed for shear strain of 50 and 150% of the rubber. By computing the characteristics of each isolator in each loading cycle, the behavior of isolator with shear plate and the LRB are compared. First, three types of isolator are compared with thicknesses and percentage of holes and steel types in shear strains of 10%, 20% and 50%, respectively. Next, the special characteristics of the isolator are compared with the LRB characteristics in shear strains of 50 and 150%. Considering the three variables at hand, the thickness and the percentage of holes and material type of shear plate, 18 different isolators are analyzed separately.

### 5.1 Effect of Shear Plate Thickness on Isolator Behavior

The PYSD1-st37 lateral force–deflection curves of the rubber bearing, assuming three different thicknesses of 2, 3 and 4 mm are shown in Fig. 8. It can be seen that the yield strength of the isolator with thicker shear plates is higher than that of the thinner plate isolator. This fact is justified by applying relations Eqs (1) and (3), which indicate the direct

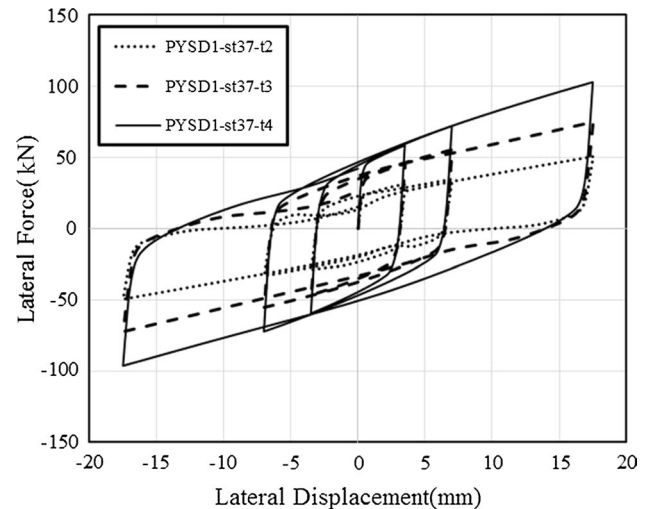


**Fig. 8** Lateral force–deflection curve of PYSD1-st37 with shear plate with different thicknesses of 2, 3 and 4 mm

relation between the yield strength and shear capacity of the plate with its thickness. Similar results are obtained in terms of the effect of shear plate thickness on the behavior of the isolators PYSD2-st37 and PYSD3-st37. The four effective horizontal stiffness properties, energy dissipation, viscous damping and the lateral force input to the PYSD1-st37, PYSD2-st37 and PYSD3-st37 isolators for 2, 3 and 4 mm thicknesses are tabulated in Tables 2, 3 and 4.

A comparison of horizontal stiffness of the isolators is observed in Fig. 9. By increasing the thickness of the plate, the effective stiffness of the isolator increases due to the direct relationship between the thickness and yield strength of the plate. For example, the effective stiffness of

**Table 2** Operational characteristics of PYSD1-st37-NRB for different thicknesses

|                              | $\gamma$ (%) | PYSD1-st37-t2 | PYSD1-st37-t3 | PYSD1-st37-t4 | LRB   |
|------------------------------|--------------|---------------|---------------|---------------|-------|
| Horizontal stiffness (kN/mm) | 10           | 8.5           | 13.6          | 16.83         | 2.26  |
|                              | 20           | 4.83          | 7.9           | 10.3          | 1.69  |
|                              | 50           | 2.85          | 4.33          | 5.7           | 1.23  |
|                              | 150          | –             | –             | –             | 0.8   |
| Dissipated energy (kJ)       | 10           | 2.91          | .45           | 0.56          | 0.074 |
|                              | 20           | 0.57          | 0.992         | 1.21          | 0.178 |
|                              | 50           | 1.36          | 2.4           | 3.19          | 0.708 |
|                              | 150          | –             | –             | –             | 2.4   |
| Viscous damping (%)          | 10           | 44            | 43            | 43            | 42    |
|                              | 20           | 38            | 40            | 38            | 34    |
|                              | 50           | 24            | 29            | 29            | 29    |
|                              | 150          | –             | –             | –             | 17    |
| Lateral force (kN)           | 10           | 31            | 45            | 58            | 7.5   |
|                              | 20           | 34            | 55            | 72            | 11.25 |
|                              | 50           | 50            | 72            | 103           | 20    |
|                              | 150          | –             | –             | –             | 43    |

**Table 3** Operational characteristics of PYSD2-st37-NRB for different thicknesses

|                              | $\gamma$ (%) | PYSD2-st37-t2 | PYSD2-st37-t3 | PYSD2-st37-t4 | LRB   |
|------------------------------|--------------|---------------|---------------|---------------|-------|
| Horizontal stiffness (kN/mm) | 10           | 7.80          | 12.7          | 16.6          | 2.26  |
|                              | 20           | 4.34          | 7.7           | 10.10         | 1.69  |
|                              | 50           | 2.57          | 3.8           | 5.40          | 1.23  |
|                              | 150          | –             | –             | –             | 0.8   |
| Dissipated energy (kJ)       | 10           | 0.28          | 0.427         | 0.53          | 0.074 |
|                              | 20           | 0.53          | 0.941         | 1.17          | 0.178 |
|                              | 50           | 1.25          | 2.22          | 3.17          | 0.708 |
|                              | 150          | –             | –             | –             | 2.4   |
| Viscous damping (%)          | 10           | 47            | 44            | 41            | 42    |
|                              | 20           | 40            | 39            | 37            | 34    |
|                              | 50           | 25            | 30            | 30            | 29    |
|                              | 150          | –             | –             | –             | 17    |
| Lateral force (kN)           | 10           | 27            | 44            | 58            | 7.5   |
|                              | 20           | 29            | 54            | 71            | 11.25 |
|                              | 50           | 46            | 65            | 96            | 20    |
|                              | 150          | –             | –             | –             | 43    |

the PYSD1-st37-t3 isolator is about 60% higher than that of the PYSD1-st37-t2 isolator in the shear strains of 10, 20, and 50%, and the effective stiffness of the PYSD1-st37-t4 isolator is about 30% higher than the PYSD1-st37-t3 isolator. As the shear strain of the isolator increases, the effective horizontal stiffness decreases due to the formation of plastic strain on the plate. The lowest effective horizontal stiffness of the isolators is related to the PYSD3-st37-2 isolator in the shear strain of 50%, which is about 49% higher than the horizontal stiffness of LRB in the shear strain of 50%.

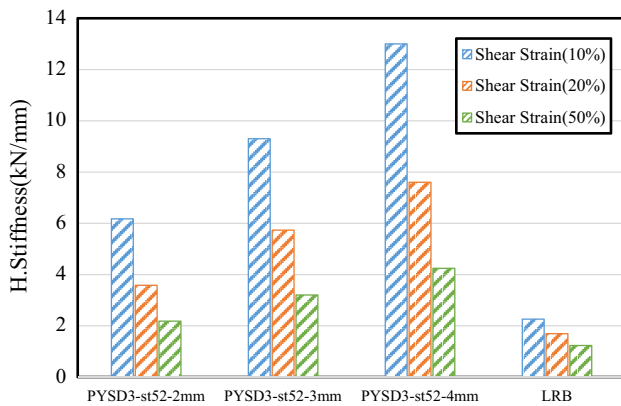
By increasing the thickness of the shear plates, the dissipated energy increases. For example, energy dissipation rate of PYSD1-st-3 isolator is about 75% higher than that

of the PYSD1-st3t-2 isolator in shear strain of 50% and the dissipated energy of PYSD1-st37-4 isolator in relation to PYSD1-st37-3 isolator in the shear strain of 50%, increases about 33%. The lowest energy dissipation related to the PYSD-st37-2 isolator is at 50% shear strain, which is about 23% higher than the LRB energy dissipation.

By comparing the results of the viscous damping of the isolators, it is observed that the viscous damping of the isolator with different thickness plates does not vary significantly, which is justified through Eq. (4). The energy dissipation and effective stiffness of the isolator with a thicker shear plate is higher than that of the isolator with a thinner shear plate. Viscous damping has a direct and inverse correlation

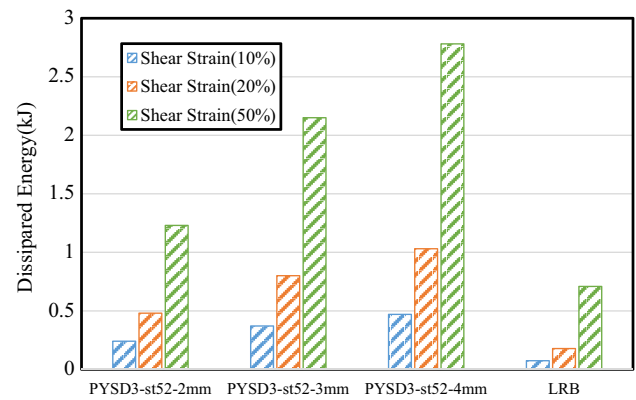
**Table 4** Operational characteristics of PYSD3-st37-NRB for different thicknesses

|                              | $\gamma$ (%) | PYSD3-st37-t2 | PYSD3-st37-t3 | PYSD3-st37-t4 | LRB   |
|------------------------------|--------------|---------------|---------------|---------------|-------|
| Horizontal stiffness (kN/mm) | 10           | 4.6           | 6.7           | 9.46          | 2.26  |
|                              | 20           | 2.76          | 4.34          | 5.77          | 1.69  |
|                              | 50           | 1.84          | 2.68          | 3.48          | 1.23  |
|                              | 150          | –             | –             | –             | 0.8   |
| Dissipated energy (kJ)       | 10           | 0.16          | 0.252         | 0.32          | 0.074 |
|                              | 20           | 0.34          | 0.540         | 0.71          | 0.178 |
|                              | 50           | 0.87          | 1.42          | 1.94          | 0.708 |
|                              | 150          | –             | –             | –             | 2.4   |
| Viscous damping (%)          | 10           | 46            | 48            | 44            | 42    |
|                              | 20           | 39            | 40            | 40            | 34    |
|                              | 50           | 24            | 27            | 29            | 29    |
|                              | 150          | –             | –             | –             | 17    |
| Lateral force (kN)           | 10           | 15            | 20            | 32            | 7.5   |
|                              | 20           | 18            | 30            | 40            | 11.25 |
|                              | 50           | 32            | 44            | 61            | 20    |
|                              | 150          | –             | –             | –             | 43    |

**Fig. 9** Effective horizontal stiffness of PYSD3-st52-NRB with different thicknesses;  $\gamma = 10\%$ ,  $20\%$  and  $50\%$ 

with energy dissipation and effective stiffness, respectively. Consequently, an increase in energy dissipation increases viscous damping while an increase in effective stiffness decreases viscous damping. As a result, viscous damping is almost identical at the specific displacement of the isolator for different thicknesses.

It is observed that the lateral force transmitted to the superstructure increases with an increase in shear strain of rubber in isolator samples with different shear plates. The thicker the shear plate, the higher the lateral force in the shear strain of the rubber bearing. The PYSD3-st37-3 isolator increases in lateral force by 38% in relation to PYSD3-st37-2 isolator and the PYSD3-st7-4 isolator increases by 40% compared to the PYSD3-st37-3 lateral force. By comparing the lateral force of the PYSD-NRBs with the LRB, the lateral force of the PYSD3-st37-3 isolator in the shear

**Fig. 10** Dissipated energy of PYSD3-st52-NRB with different thicknesses;  $\gamma = 10\%$ ,  $20\%$  and  $50\%$ 

strain of 50% of the rubber is approximately the same as that of a LRB in the shear strain of 150% of the rubber. Similar results are obtained for the effective horizontal stiffness, dissipated energy, viscous damping and the lateral force for PYSD-st52 isolators. The effect of plate thickness on the PYSD3-st52 isolator behavior is observed in Figs. 9, 10, 11 and 12.

## 5.2 Effect of Shear Plate Holes on Isolator Behavior

The PYSD-st37-t2 isolator lateral force–deflection curve for three different types of perforated shear plates with a thickness of 2 mm is shown in Fig. 13. By comparing the results of the effective stiffness of the isolators according to Fig. 14, the effective stiffness of the PYSD1-st37-t3 and PYSD2-st37-t3 isolators is not significantly different



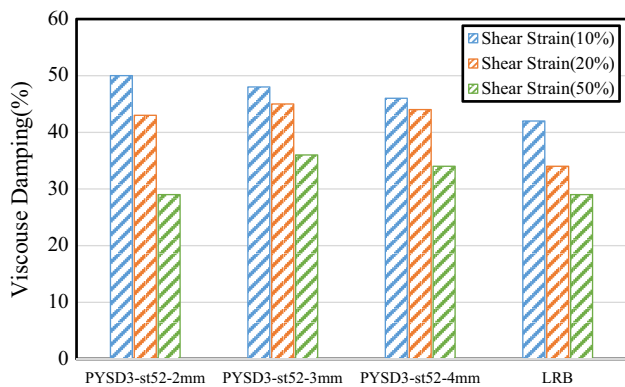


Fig. 11 Equivalent viscous damping of PYSD3-st52-NRB with different thicknesses;  $\gamma = 10\%$ ,  $20\%$  and  $50\%$

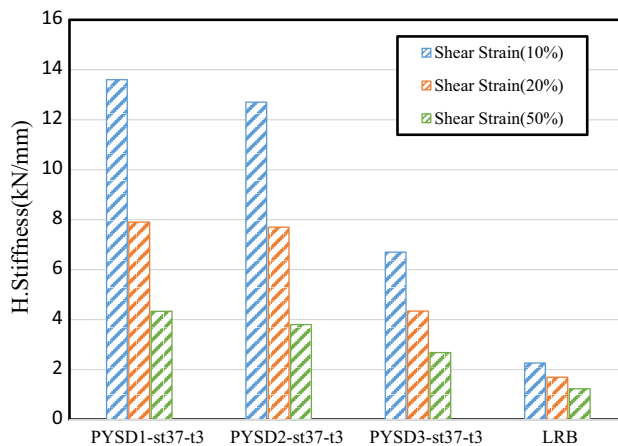


Fig. 14 Effective horizontal stiffness of PYSD-st37-t3-NRB for three different types of perforated shear plate;  $\gamma = 10\%$ ,  $20\%$  and  $50\%$

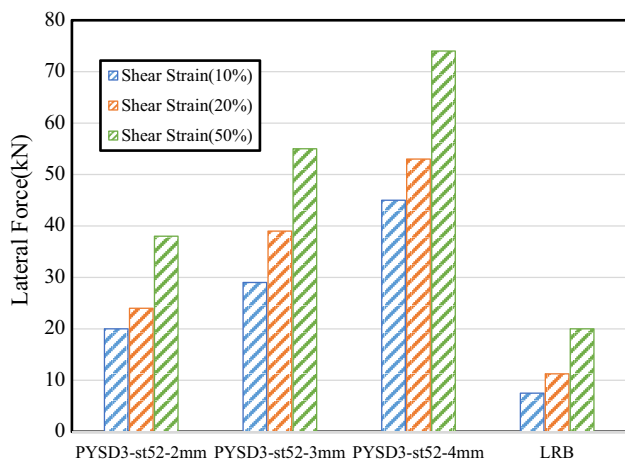


Fig. 12 Lateral force of PYSD3-st52-NRB with different thicknesses;  $\gamma = 10\%$ ,  $20\%$  and  $50\%$

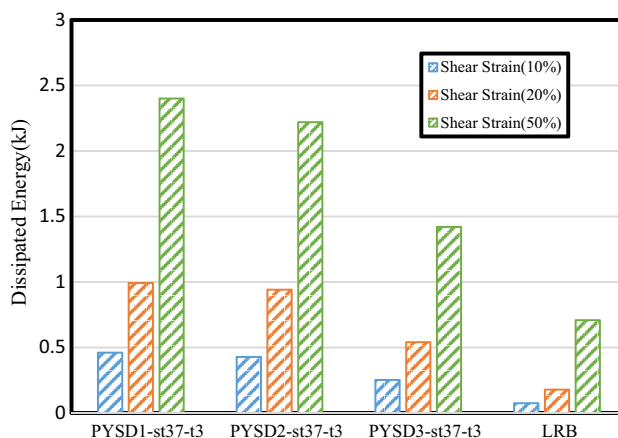


Fig. 15 Dissipated energy of PYSD-st37-t3-NRB for three different types of perforated shear plate;  $\gamma = 10\%$ ,  $20\%$  and  $50\%$

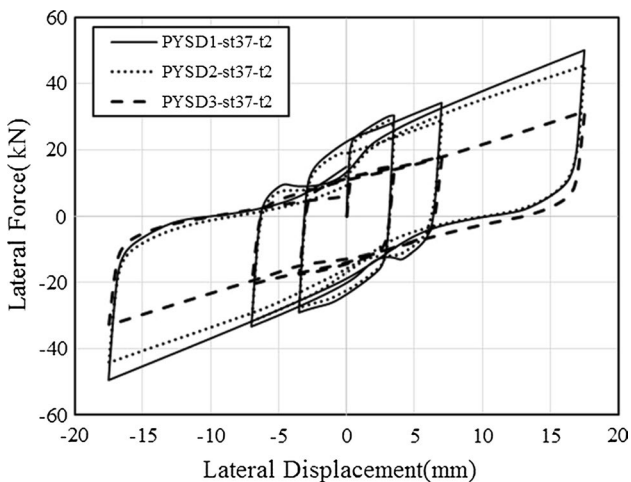


Fig. 13 Lateral force—deflection curve of PYSD-st37-t2-NRB for three different types of perforated shear plates

due to the low difference in the perforated section of the two shear plates. However, the effective stiffness of the PYSD3-st37-t3 isolator is decreased by about 40% in relation to the stiffness of the PYSD2-st37-t3 isolator at 50% shear strain. The least effective stiffness of the isolators is due to the PYSD3-st37-t2 isolator at 50% shear strain, which is about 49% higher than the effective stiffness of the LRB at 50% shear strain.

The energy dissipation of isolators decreases by an increase in perforation of the shear plate (Fig. 15). In this case, because of the approximate uniformity of the perforation section of PYSD1 isolators and PYSD2 isolators, the energy dissipation is not significantly different. In the PYSD3 isolator, due to a significant increase in the perforated section of the shear plates, compared with the other two isolators, significant energy dissipations are noticeable compared to the other two isolators. The PYSD3-st37-t3

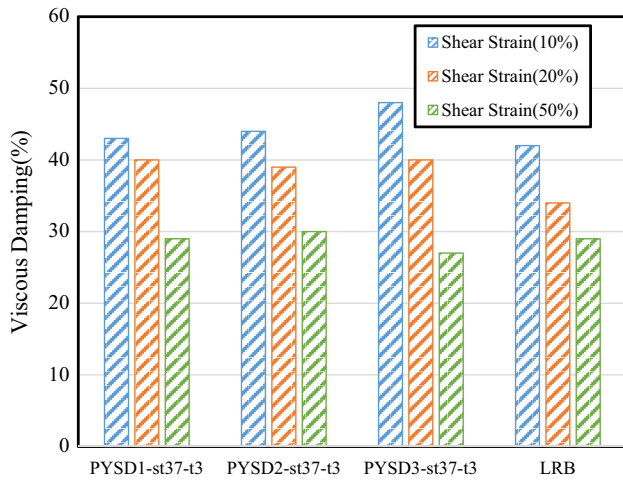


Fig. 16 Equivalent viscous damping of PYSD-st37-NRB for three different types of perforated shear plate;  $\gamma = 10\%$ ,  $20\%$  and  $50\%$

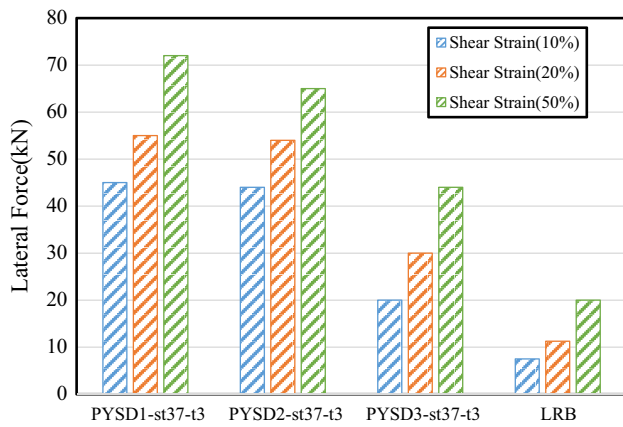


Fig. 17 Lateral force of PYSD-st37-NRB for three different types of perforated shear plate;  $\gamma = 10\%$ ,  $20\%$  and  $50\%$

isolator in comparison with the PYSD1-st37-t3 isolator at 50% shear strain, indicate a decrease of about 70%.

By considering an increase in cross-sectional area of the holes, the effective stiffness of the isolator, which is of inverted viscous damping ratio, decreases and the energy dissipation, which is directly proportional to viscous damping decreases; thus, the viscous damping does not change significantly with the increase of the perforation of the shear plates (Fig. 16). Viscous damping of PYSD3-st37-t4 isolator with viscous damping of LRB at 50% shear strain are equal.

The lateral force transmitted to superstructure decreases with an increase in the perforation of the shear plates (Fig. 17). This reduction value is justified by the reduction coefficient  $(1 - \frac{A}{A_0})$  for plate shear capacity according to Eq. (3). The minimum lateral force at 50% shear strain of the PYSD3-st37-t2 is 32 kN.

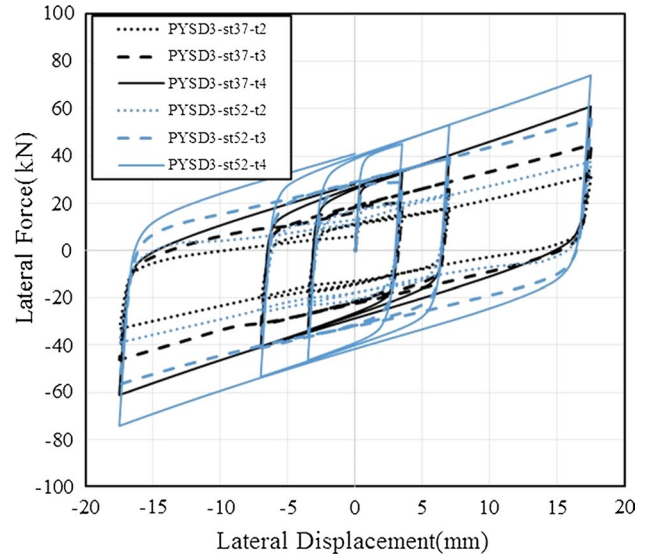


Fig. 18 Lateral force—deflection curve of PYSD3-NRB with shear plate with different material and different thickness

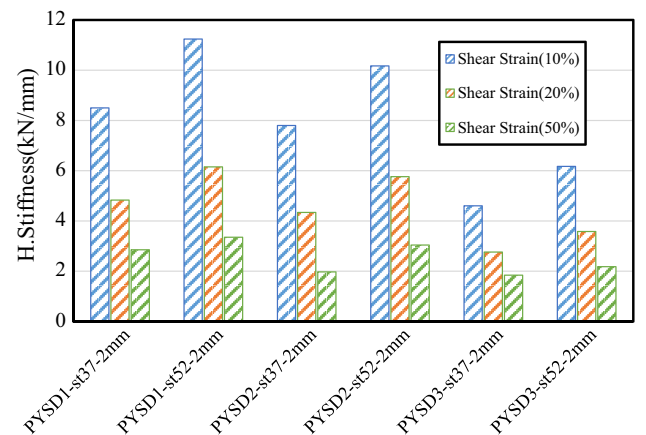


Fig. 19 Effective horizontal stiffness of PYSD-t2-NRB for different material of shear plate;  $\gamma = 10\%$ ,  $20\%$  and  $50\%$

### 5.3 The Effect of the Shear Plate Material Type on Isolator Behavior

The PYSD3 isolators are modeled and illustrated by st37 and st52 for shear plates (Fig. 18). The effective stiffness of the isolators made of st52 are compared to that of st37. Where, it is revealed at low strain st52 is of a higher effective stiffness. Since the shear yield strength of the plate is proportional to tensile yield stress in accordance with Eq. (1), an increase in the effective stiffness of the isolator is justified by an increase in the tensile yield stress. The effective stiffness of isolators with a thickness of 2 mm for shear plate made of steel st37 and st52 are shown in Fig. 19.

The energy dissipation of the PYSD-st52 isolator is significant compared to that of the PYSD-st37 isolator. The energy dissipation of PYSD3-st52-t3 isolator is about 50% higher than that of the PYSD3-st37-t3 isolator (Fig. 20).

Although a change in plate thickness and the variation in the perforation of the shear plates is of little effect on the viscous damping, a change in plate material is affected by the viscous damping. For example, the equivalent viscous damping of PYSD3-st52-t3 isolator is about 50% higher than the PYSD3-st37-t3 isolator (Fig. 21). An increase in the dissipating energy by changing the plate material is more than the increase in the stiffness of shear plate. Since viscous damping is directly related to the energy dissipation and inversely related to stiffness, the greater dissipating energy leads to an increase in the viscous damping of isolator.

The lateral force transmitted to superstructure for the PYSD-st52 isolator increases compared to that of the PYSD-st37 isolator (Fig. 22). For example, the lateral force of the PYSD3-st52-t3 isolator is about 23% higher than that of the PYSD3-st37-t3 isolator in the 50% shear strain.

### 6 Conclusion

In this paper, performance of an innovative perforated yielding shear device isolator is assessed. In this isolator, the lead core in rubber bearing is replaced by the perforated yielding shear plates as an energy dissipated device. One of the advantages of rubber bearing with shear plates in relation to the LRB is its easy manufacturing process, placement, replacement. Another advantage of this isolator is the ability to dissipate energy in a smaller displacement than that of LRB. Isolators are compared with different plate thicknesses, hole area percentage and steel type at shear strains of

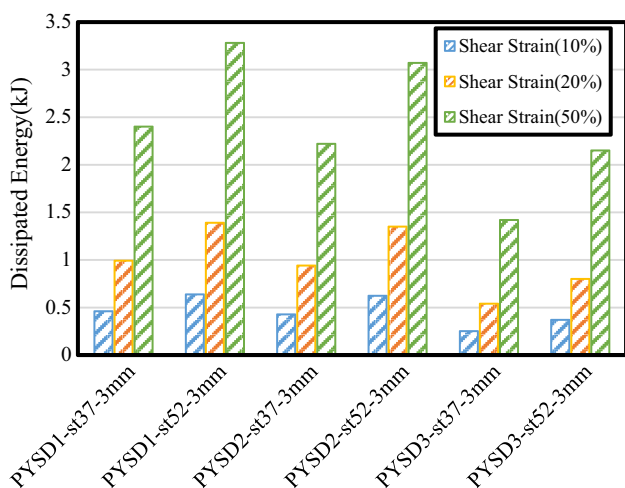


Fig. 20 Dissipated energy of PYSD-t3-NRB for different material of shear plate;  $\gamma = 10\%$ ,  $20\%$  and  $50\%$

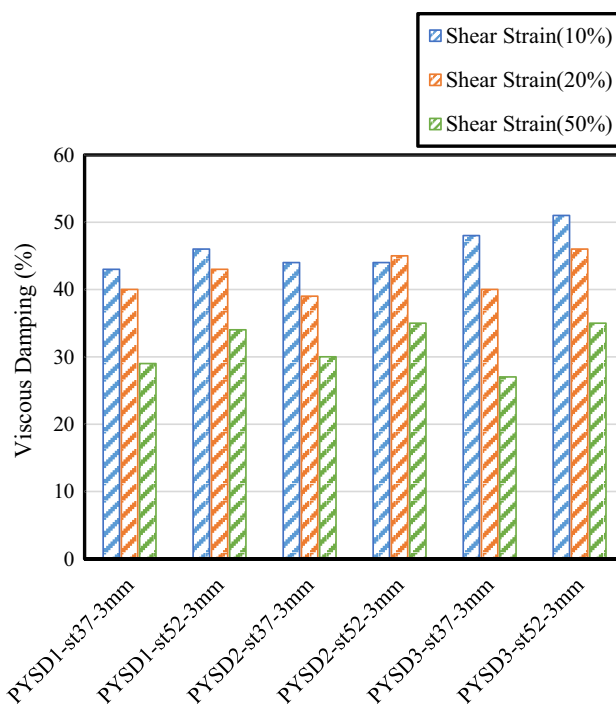


Fig. 21 Equivalent viscous damping of PYSD-t3-NRB for different material of shear plate;  $\gamma = 10\%$ ,  $20\%$  and  $50\%$

10%, 20% and 50%. The special characteristics of this newly developed isolator are compared with the LRB characteristics at shear strains of 50% and 150%.

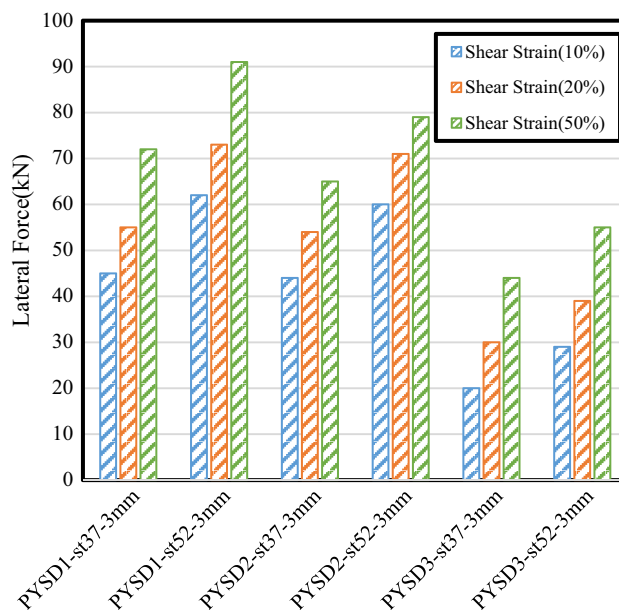


Fig. 22 Lateral force of PYSD-t3-NRB for different material of shear plate;  $\gamma = 10\%$ ,  $20\%$  and  $50\%$

The following are considered as the outcome of this study:

1. By increasing the thickness of the plate, the effective stiffness, dissipated energy and lateral force of the isolator increase due to the direct correlation between the thickness and yield strength of the plate. It is observed that the viscous damping of the isolator with different plate thicknesses does not vary significantly. The lowest energy dissipation and horizontal stiffness related to the PYSD-st37-t2 isolator at 50% shear strain are about 50 and 23% higher than that of the LRB. PYSD3-st37-t3 lateral force at 50% shear strain is the same with the LRB lateral force at 150% shear strain. With regard to the acceptable dissipated energy of the shear plate isolator at 50% shear strain, it can be concluded that the function of this isolator is appropriate compared to the LRB at 150% shear strain.
2. By increasing the perforation of the shear plate, the effective stiffness, dissipated energy and lateral force of the isolator decrease, with a slight change in viscous damping. Movement ability of isolator is an important issue. Due to high percentage of holes area of PYSD3, the displacement of the isolator is much higher than that of two other isolators with less holes area. By comparing the isolators in terms of percentage of perforated plate, the PYSD3-st37-t3, in addition to the proper displacement, has sufficient energy dissipation, with acceptable lateral force.
3. When yield stress of shear plate changes from st37 to st52 steel types, the effective horizontal stiffness, the dissipated energy, viscous damping and the lateral force increase. The amount of dissipated energy of PYSD-st52 isolators is higher than that of the PYSD-s37 isolators, which is noticeable in comparison with the change in plate thickness and perforation percentage. Because viscous damping has a direct correlation with dissipated energy, changing yield stress of shear plate from st37 to st52 leads to an increase in viscous damping. The PYSD3-st52-t3 dissipated energy and viscous damping ratio is about 50 and 30% higher than that of the PYSD3-st37-t3, respectively.
4. The PYSD3-st37-t3 outperforms other isolators. Although the amount of energy dissipation at 50% shear strain is about 70% lower than LRB at 150% shear strain but viscous damping is 60% higher. The PYSD3-st37-t3 lateral force at 50% shear strain is the same as LRB lateral force at 150% shear strain. In the PYSD3-st52-t3, the energy dissipation at 50% shear strain is approximately equal to that of LRB at 150% shear strain. The amount of lateral force transferred to the superstructure is about 25% higher.
5. Although this study shows the capability of using perforated yielding shear device in isolators, experimental evaluation is needed to prove its practical application. Also due to the limitation of shear strain in this type of isolator, design basics of this type should be defined differently rather than LRB.

## References

- Abe, M., Yoshida, J., & Fujino, Y. (2004). Multiaxial behaviors of laminated rubber bearings and their modeling. I: Experimental study. *Journal of Structural Engineering*, 130(8), 1119–1132.
- Ahn, H. J., Kim, Y. J., & Bae, J. H. (2016). Cyclic loading test of wall damping system with steel dampers. *Advances in Structural Engineering*, 19(8), 1262–1274.
- Asl, M. J., Rahman, M., & Karbakhsh, A. (2014). Numerical analysis of seismic elastomeric isolation bearing in the base-isolated buildings. *Open Journal of Earthquake Research*, 3(01), 1.
- Bhuiyan, A., Okui, Y., Mitamura, H., & Imai, T. (2009). A rheology model of high damping rubber bearings for seismic analysis: Identification of nonlinear viscosity. *International Journal of Solids and Structures*, 46(7), 1778–1792.
- Chan, R. W., Albermani, F., & Kitipornchai, S. (2013). Experimental study of perforated yielding shear panel device for passive energy dissipation. *Journal of Constructional Steel Research*, 91, 14–25.
- Chan, R. W., Albermani, F., & Williams, M. S. (2009). Evaluation of yielding shear panel device for passive energy dissipation. *Journal of Constructional Steel Research*, 65(2), 260–268.
- De Matteis, G., Sarracco, G., & Brando, G. (2016). Experimental tests and optimization rules for steel perforated shear panels. *Journal of Constructional Steel Research*, 123, 41–52.
- Dezfuli, F. H., & Alam, M. S. (2013). Shape memory alloy wire-based smart natural rubber bearing. *Smart Materials and Structures*, 22(4), 045013.
- Dezfuli, F. H., & Alam, M. S. (2015). Hysteresis model of shape memory alloy wire-based laminated rubber bearing under compression and unidirectional shear loadings. *Smart Materials and Structures*, 24(6), 065022.
- Dezfuli, F. H., & Alam, M. S. (2017). Smart lead rubber bearings equipped with ferrous shape memory alloy wires for seismically isolating highway bridges. *Journal of Earthquake Engineering*, 22, 1–26.
- Dezfuli, F. H., Li, S., Alam, M. S., & Wang, J. Q. (2017). Effect of constitutive models on the seismic response of an SMA-LRB isolated highway bridge. *Engineering Structures*, 148, 113–125.
- Formisano, A., Lombardi, L., & Mazzolani, F. (2016). Perforated metal shear panels as bracing devices of seismic-resistant structures. *Journal of Constructional Steel Research*, 126, 37–49.
- Ge, H., Chen, X., & Kang, L. (2012). Demand on stiffened steel shear panel dampers in a rigid-framed bridge pier under repeated seismic ground motions. *Advances in Structural Engineering*, 15(3), 525–546.
- Ghobarah, A., & Ali, H. (1990). Seismic design of base-isolated highway bridges utilizing lead-rubber bearings. *Canadian Journal of Civil Engineering*, 17(3), 413–422.
- Iizuka, M. (2000). A macroscopic model for predicting large-deformation behaviors of laminated rubber bearings. *Engineering Structures*, 22(4), 323–334.
- Naeim, F., & Kelly, J. M. (1999). *Design of seismic isolated structures: from theory to practice*. Hoboken, NJ: Wiley.

- Oh, S. H., Song, S. H., Lee, S. H., & Kim, H. J. (2013). Experimental study of seismic performance of base-isolated frames with U-shaped hysteretic energy-dissipating devices. *Engineering Structures*, 56, 2014–2027.
- Paul, D. (2016). Effect of lead in elastomeric bearings for structures located in seismic region. *Procedia Technology*, 25, 146–153.
- Purba, R., & Bruneau, M. (2009). Finite-element investigation and design recommendations for perforated steel plate shear walls. *Journal of Structural Engineering*, 135(11), 1367–1376.
- Roberts, T. M., & Sabouri-Ghomi, S. (1992). Hysteretic characteristics of unstiffened perforated steel plate shear panels. *Thin-Walled Structures*, 14(2), 139–151.
- Ryan, K. L., Kelly, J. M., & Chopra, A. K. (2005). Nonlinear model for lead-rubber bearings including axial-load effects. *Journal of engineering mechanics*, 131(12), 1270–1278.
- Sanchez, J., Masroor, A., Mosqueda, G., & Ryan, K. (2012). Static and dynamic stability of elastomeric bearings for seismic protection of structures. *Journal of Structural Engineering*, 139(7), 1149–1159.
- Toopchi-Nezhad, H., Tait, M. J., & Drysdale, R. G. (2008). Testing and modeling of square carbon fiber-reinforced elastomeric seismic isolators. *Structural Control and Health Monitoring*, 15(6), 876–900.
- Valizadeh, H., Sheidaii, M., & Showkati, H. (2012). Experimental investigation on cyclic behavior of perforated steel plate shear walls. *Journal of Constructional Steel Research*, 70, 308–316.
- Vian, D., Bruneau, M., Tsai, K. C., & Lin, Y. C. (2009). Special perforated steel plate shear walls with reduced beam section anchor beams. I: Experimental investigation. *Journal of Structural Engineering*, 135(3), 211–220.
- Warn, G. P., & Ryan, K. L. (2012). A review of seismic isolation for buildings: historical development and research needs. *Buildings*, 2(3), 300–325.
- Williams, M. S., & Albermani, F. (2003). *Monotonic and cyclic tests on shear Diaphragm dissipators for steel frames*. Civil Engineering Research Bulletin No. 23, University of Queensland, Australia.